A proposal of a technique for correlating defect dimensions to vibration amplitude in bearing monitoring

A Proposal of a Technique for Correlating Defect Dimensions to Vibration Amplitude in Bearing Monitoring

Eugenio Brusa[1], Fabio Bruzzone[1], Cristiana Delprete[1], Luigi Gianpio Di Maggio[1] and Carlo Rosso[1]

[1]*Politecnico di Torino, Corso Duca degli Abruzzi, 24, 10129, Torino, Italy*

eugenio.brusa@polito.it
fabio.bruzzone@polito.it
cristiana.delprete@polito.it
luigi.dimaggio@polito.it
carlo.rosso@polito.it

ABSTRACT

The capability of early stage detection of a defect is gaining more and more importance because it can help the maintenance process, the cost reduction and the reliability of the systems.

The increment of vibration amplitude is a well-known method for evaluating the damage of a component, but it is sometimes difficult to understand the exact level of damage. In other words, the amplitude of vibration cannot be directly connected to the dimension of the defect.

In the present paper, based on a non-Hertzian contact algorithm, the spectrum of the pressure distribution in the contact surface between the race and the rolling element is evaluated. Such spectrum is then compared with the acquired spectrum of a vibration response of a defected bearing. The bearing vibration pattern was previously analyzed with monitoring techniques to extract all the damage information.

The correlation between the spectrum of the pressure distribution in the defected contact surface and the analyzed spectrum of the damaged bearing highlights a strict relationship. By using that analysis, a precise correlation between defect aspect and dimension and vibration level can be addressed to estimate the level of damaging.

1. INTRODUCTION

Over the past twenty years, many research projects have been devoted to the development of predictive maintenance techniques in rotating machinery. This is also known as Condition-Based Monitoring (CBM). The economic benefits of CBM related to lower maintenance costs, fewer machine failures and increased production are appreciable in the long run and repay extra costs due to the initial investment (Mohanty, 2014). Indeed, predictive maintenance requires appropriate sensors and acquisition systems. The concepts of health indicators and Remaining Useful Life (RUL) are central to the research on CBM (Wang, Tsui and Miao, 2018). Namely, the construction of health indicators is the key feature for the monitoring and the prediction of the conditions and RUL of machines while in operation. Lubricant analysis and vibration analysis are the two most common techniques used in CBM for the construction of health indicators. The second is the prevalent method since it reacts immediately to change and can be adopted in conjunction with powerful signal processing techniques. These are able to emphasize faults from mixed signals which carry information of several machine components (e.g. gears, bearings, unbalances, misalignments). Conversely, a considerable amount of time passes between data acquisition and processing in oil analysis, though online systems exist (Randall, 2011). In vibration-based condition monitoring (VBCM), diagnostic information are extrapolated from vibration signal by means of accelerometers and acoustic emission (AE) and processed in time, frequency and time-frequency domain (Randall & Antoni, 2011).

Of particular concern is the health monitoring of rolling element bearings. These are among the most critical components in rotating machinery since their failure promotes the breakdown of the neighboring components. Moreover, they affect dynamic behavior and stability of rotating systems (Genta, 2007; Genta, Delprete and Brusa, 1999). For this reason, early fault detection in bearings plays a crucial role in the health monitoring of the whole mechanical system. Actually, bearing vibrations are associated to various statistically independent components which mix up and then result in the acquired signal. The

separation of periodic from random components and, then, of stationary from non-stationary contributions involves Blind Source Separation (BSS) (Antoni, 2005; Antoni & Braun, 2005), fundamental device for the enhancement of bearing signal. In this context, mechanical signal processing proves to be a robust tool since many characteristic features can be recognized in faulty bearing signals. For instance, several authors (Mauricio, Smith, Randall, Antoni and Gryllias, 2018; McCormick & Nandi, 1998; Randall, 2011; Randall, Antoni and Chobsaard, 2001; Randall & Antoni, 2011) emphasized that, given the random slip occurring in rolling elements, the acceleration signal resulting from bearings with localized faults has to be considered cyclostationary, that is with non-constant (periodic) statistical features. Thus, it can be differentiated from gears signal which is always deterministic. In this case, the signal spectrum is characterized by discrete frequency components as long as angular resampling (Bonnardot & Randall, 2004; Guo, Liu, Na and Fung, 2012; McFadden, 1989; Potter & Gribler, 1989) is adopted to avoid smearing of shaft speed components. Angular resampling is also known in literature as *order tracking*. Furthermore, signals generated by faulty bearings are characterized by the striking of rolling elements on the defected inner or outer race. Bursts excite high frequency resonances. Consequently, the diagnostic information linked to the ball passing frequencies is not directly accessible neither in the raw signal nor in its spectrum, typically obtained by means of Fast Fourier Transform algorithm (FFT). Envelope analysis overcomes limitations imposed by the raw spectrum content. This technique was developed almost four decades ago with the name of High Frequency Resonance Technique (HFRT) (Burchill, John and Wilson, 1973; Burchill, 1973; Darlow & Badgley, 1975; Harting, 1978; McFadden & Smith, 1984a, 1984b) and it aimed to shift Fourier analysis from the high resonant frequencies range to the lower one of faults (Randall & Antoni, 2011). Envelope analysis takes advantage of Hilbert transform (Bendat, 1991) for digital signal filtering. It is able to highlight carrier and modulating frequencies in amplitude modulated signals. Such demodulation is very powerful in the bearing signal processing. Actually, the spectra of demodulated bearing signals show fault frequencies with sidebands spaced by shaft speed frequency. In relation to the position of the defect, different fault frequencies can be recognized. Ball passing frequency on the outer race (*BPFO*), on the inner race (*BPFI*) and the Fundamental Train Frequency (*FTF*), that is cage speed, are described by the following kinematic relations (Randall, 2011).

$$BPFO = \frac{nf_r}{2}\left(1 - \frac{d}{D}cos(\Phi)\right) \qquad (1)$$

$$BPFI = \frac{nf_r}{2}\left(1 + \frac{d}{D}cos(\Phi)\right) \qquad (2)$$

$$FTF = \frac{f_r}{2}\left(1 - \frac{d}{D}cos(\Phi)\right) \qquad (3)$$

where f_r is the rotation frequency, n the number of rolling elements, Φ the load angle, and d the diameter of rolling element and D the distribution diameter.

Studies over the past two decades provided important information on the choice of the optimal demodulation frequency band. In this context, time-frequency analysis emerges as an effective device as explained by the following. Frequency analysis and FFT decompose signals by using base functions localized in the frequency domain but not in the time domain. Nevertheless, faulty bearings are characterized by impulsive and time-localized phenomena. The Short Time Fourier Transform (STFT), reported in Eq. (4), and the Wavelet Transform, being essentially based on sliding windows $w(t-\tau)$, are able to localize harmonic contributions even in time. This fundamental property finds a wide range of application in time-frequency analysis.

$$X(f,\tau) = \\ = \int_{-\infty}^{+\infty} x(t)w(t-\tau)e^{-j2\pi ft}dt \qquad (4)$$

It is beyond the scope of this study to analyze limitations of STFT with respect to multi-resolution analysis (Akansu, P.A. Haddad, P.R. Haddad, 2001) offered by Wavelets, especially in the high frequency range, though the authors are aware of this research branch. These transforms can both be used to extract the Spectral Kurtosis (SK) of Eq. (5) (Randall, 2011) and the Fast Kurtogram (FK) (Fig. 1). Time averaging is indicated by $\langle\cdot\rangle$.

$$K(f) = \frac{\langle |X(f,t)|^4 \rangle}{\langle |X(f,t)|^2 \rangle^2} - 2 \qquad (5)$$

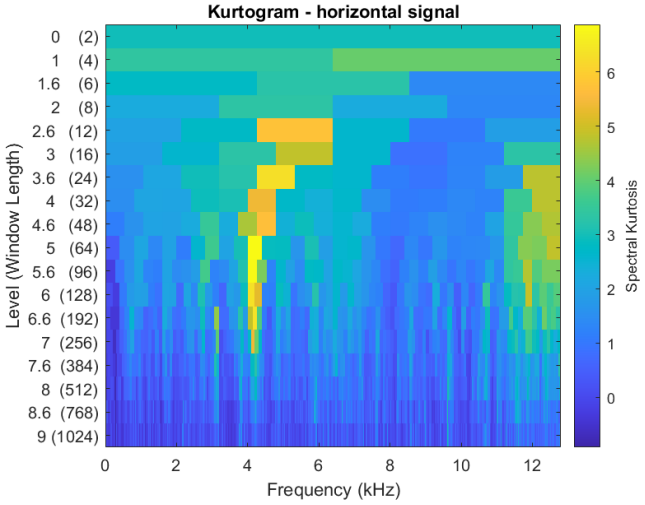

Figure 1. Fast Kurtogram for the choice of the optimal demodulation band and window length.

In the latter, frequency bands with the highest Kurtosis, established by extensive literature as an indicator of impulsiveness (Antoni, 2007, 2007, 2015; Antoni & Randall, 2006; Borghesani, Pennacchi and Chatterton; 2014, Wang, Tse and Tsui, 2013), can be found. The kurtogram of Fig. 1 is obtained by calculating the SK through the fast kurtogram algorithm for different window sizes. In this way, the signal content strictly related to impulsiveness is accentuated. Moreover, frequency bands underlined by the aforementioned fourth-order statistics are comparable with those accentuated by the difference between dB spectra of damaged and undamaged bearings (Randall, 2011; Randall & Antoni, 2011). In the latter case, second order statistics and Power Spectral Densities (PSD) computed by Welch method (Welch, 1975) are employed. Differently from SK methods, this requires machine signature to be known. Actually, prior to the establishment of SK and FK techniques, the PSD method was mostly used. Then, a considerable amount of literature has been published on Wavelets applications in bearing signal processing (Hong & Liang, 2009; Kankar, Sharma and Harsha, 2011; Lin & Qu, 2000; Peng & Chu, 2004; Rubini & Meneghetti, 2001; Shao, Jiang, F. Wang and Y. Wang, 2017; Tabrizi, Garibaldi, Fasana and Marchesiello, 2015b; Wang, Makis and Yang, 2010). In particular, Wavelets denoising (Donoho & Johnstone, 1994; Qiu, Lee, Jin & Yu, 2006; Wang et al. 2013) can be considered an alternative to SK methods to enhance bearing signal. In the present work, different Wavelet denoising methods were applied but they showed to be not successful as much as FK (Fig. 2). Indeed, Fig. 2 shows that the Kurtosis of the denoised signal is very slightly modified by Wavelet denoising.

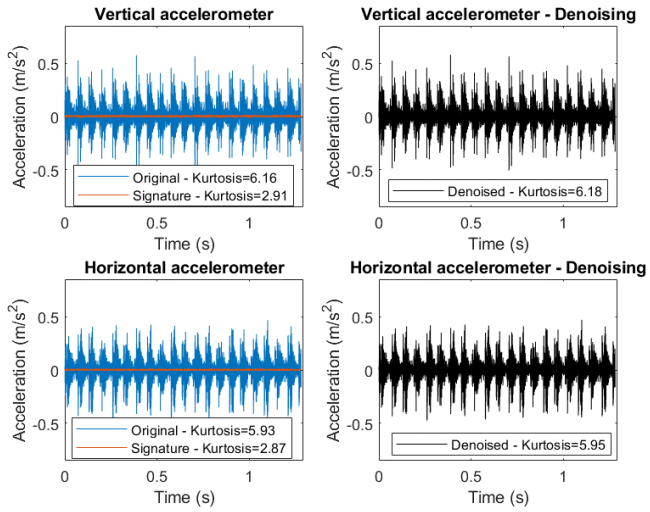

Figure 2. Wavelet denoising in the acquired signal (Bayesian method).

Extensive research has shown envelope analysis to be a powerful tool in bearings diagnostic (Delprete, Milanesio and Rosso, 2005, 2020; Guo et al. 2012; Rubini & Meneghetti, 2001; Sawalhi, 2007; Sawalhi & Randall, 2008; Yu, Cheng and Yang, 2005). However, recent works have established the effectiveness of data-driven models in CBM (Baccarini, Rocha e Silva, de Menezes and Caminhas, 2011; Ben Ali, Saidi, Mouelhi, Chebel-Morello and Fnaiech, 2015, Herp, Ramezani, Bach-Andersen, Pedersen and Nadimi, 2018; Liu, Cao, Chen, He and Shen, 2013; Pinheiro, Brandao and Da Costa, 2019; Shao, Jiang, F. Wang, Y. Wang, 2017; Tabrizi, Garibaldi, Fasana, Marchesiello, 2015a; Widodo & Yang, 2007). Indeed, machine learning algorithms, such as Support Vector Machine (SVM), can be used to construct health indicators based on probabilistic and statistical features. For instance, Mahalanobis distance (Daga, Fasana, Marchesiello and Garibaldi, 2019; Jin, Wang, Chow and Sun, 2017; Shakya, Kulkarni and Darpe, 2015) was applied by Jin et Chow (2013) in fault classification for cooling fan. These approaches are intrinsically different from quasi-deterministic methods such as envelope analysis since classifiers and thresholds are built on the base of collected data. Because of this fact, a large amount of data for training and validation is required. Despite the indisputable effectiveness of these methods, their link with the analyzed physical phenomena is weaker than envelope-based methods which mostly rely on the physical considerations about cyclostationarity and amplitude modulation.

The challenge of defect detection in CBM joins the one of defect size estimation. In this regard, some of the previous works have considered AE analysis (Al-Dossary, Hamzah, Mba, 2009; Al-Ghamd & Mba, 2006; Mba, 2008), whereas others devoted to the study of spalls size by using vibration signals (Chen & Kurfess, 2018).

The present study aims to contribute to this growing area of research by exploring the relation between health indicators extrapolated from envelope analysis and the size of localized defects in rolling bearings. Namely, the harmonic contribution given by the first fault characteristic frequency in the spectrum is compared with the same quantity obtained from the contact pressure signal. This signal results from non-Hertzian contact simulations run for the defected bearing. The contact pressure signal is, indeed, supposed to contain the information about defect size. Therefore, it is used in this work to overcome limitations related to the lack of different acquisitions for different defect sizes.

2. MATERIALS AND METHODS

The current investigation involved experimental, numerical and signal processing activities. The first is related to the extraction of vibration signal from the damaged and the undamaged bearing. The second refers to the numerical solution of the non-Hertzian contact model used for the estimation of the contact pressure. Finally, the third is connected to envelope analysis, previously introduced as one of the most well-known tools for assessing bearings

health conditions. The aim of this analysis is to correlate health indicators with damage severity. In particular, the energetic contribution relative to *BPFI* harmonics is proposed as a marker for defect size estimation.

2.1. Experimental investigation

The experimental test rig (Fig. 3) consists of an asynchronous three-phase electric motor which drives the motion of a pulley through a trapezoidal belt. The rig is equipped with a manual screw-nut pretension system. The pulley is fitted on a shaft supported by the tested bearings. Thanks to this simple as much as realistic experimental set up, different faulty states can be analyzed (e.g. inner or outer race defect, overload, belt misalignment, lubricant contamination) by building frameworks which retrace typical operation conditions of industrial machines. The main characteristics of the test rig are reported in Table 1. The test refers to continuous operation conditions at ambient temperature.

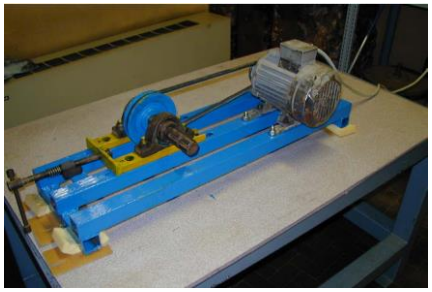

Figure 3. Experimental test rig.

Table 1. Test rig characteristics.

Asynchronous three-phase electric motor	
Power [kW]	0.75
cosφ	0.79
Speed [rpm]	1400
Voltage	220 V Δ - 380 V Y
Current	3.4 A Δ - 1.95 A Y
Pulleys	
Driving Pulley	Di=51 mm De=78 mm
Driven Pulley	Di=77 mm De=106 mm
Tested Bearings	
2x SKF YAR 206-2F	
BPFO [Hz]	56.7
BPFI [Hz]	85.6
FTF [Hz]	6.0
ω [rpm]	947.8
Test rig natural frequencies	
1 natural frequency	300 Hz
2 natural frequency	1850 Hz
3 natural frequency	5800 Hz

The experimental tests were carried out by placing two accelerometers PCB 308B of type ICP (Table 2) on the bearing case to study both radial and axial vibrations. The first accelerometer was threaded in the vertical direction perpendicular to the shaft axis, whereas the second was positioned along the direction of the shaft axis by means of a magnetic base. This choice is justified by the fact that, in an industrial context, it is not always possible to use threaded connections. Sensors were connected to DIFA-APB 200 signal analyzer.

Prior to the data acquisition, the impulse response of the structure was measured to estimate the structural resonances of the test rig. Then, a sharp edge tool was used to introduce a defect on the inner race of the bearing. The size of the wedge-shaped defect was comparable with the material roughness (1.6 μm) to simulate fault initiation. Finally, signals were acquired (Table 3 and Fig. 2) and the one-sided FFT was applied for the computation of the spectra (Fig. 4). The tests were carried out measuring rotation speed by means of a tachometer.

Table 2. Accelerometer characteristics.

Accelerometers PCB 308B	
Voltage sensitivity [mV/(m/s^2)]	10.2
Frequency range (+/–5%) [Hz]	1-3000
Frequency range (+/–10%) [Hz]	0.7-6500
Resonant frequency [kHz]	>22
Amplitude range [+/- m/s^2 pk]	490
Resolution (Broadband) [m/s^2 rms]	0.0098
Temperature range [°C]	–54 to 121
Amplitude linearity [%]	+/– 1

Table 3. Signal acquisitions.

T - duration of the acquisition [s]	1.28
Fs - sampling frequency [kHz]	2.56
N - number of samples	32768

The same analysis was performed for the axial accelerometer, but significative differences were not found in the harmonic contributions. As emphasized in Fig. 4, the first test rig resonance was excited by the 19th harmonic of the shaft speed.

2.2. Contact pressure analysis

The contact pressure distribution in the defected inner race was calculated by using a Matlab® code developed to solve a frictionless non-Hertzian contact problem in a two-dimensional space. The contact conditions reported in Eq. (6) were defined by the Hertz-Signorini-Moreau problem (Johnson, 1987; Kalker, 2013; Wriggers, 2002).

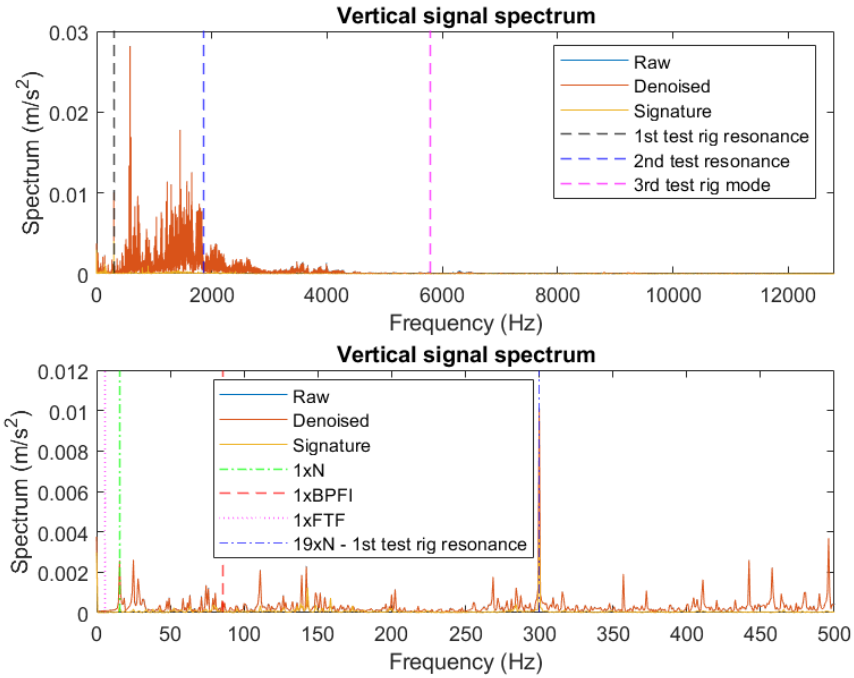

Figure 4. FFT spectrum of the acquired signal.

$$\begin{cases} \boldsymbol{h} \geq 0 \\ \boldsymbol{p_n} \geq 0 \\ \boldsymbol{h} \cdot \boldsymbol{p_n} = 0 \end{cases} \qquad (6)$$

Bolted variables represent vectors and matrices. The first condition prevents surface penetration by constraining the gap function $\boldsymbol{h}$, the second ensures the normal contact pressure $\boldsymbol{p_n}$ to be positive in the contact area whereas, thanks to the third condition, $\boldsymbol{p_n}$ is imposed to be null on the outside from the contact area ($\boldsymbol{h} = \boldsymbol{0}$).

The elastic deformation thus resulting is expressed by means of the matrix $\boldsymbol{C}$, containing the influence coefficient associated to the elastic properties of the contact surfaces:

$$\boldsymbol{\delta} = \boldsymbol{C} \cdot \boldsymbol{p_n} \qquad (7)$$

A square-based and wedge-shaped defect was introduced in the mesh of the inner race to simulate damage initiation. The height of the defect was equal to the square dimensions in order to identify a single dimension for the characterization of the simulated defect.

The code was run for characteristic defect sizes of 6, 20, 50 and 100 µm and the resulting maximum contact pressure was extracted as a function of the rotation angle. Fig. 5 shows the contact pressure distribution and the maximum contact pressure pattern for a 50 µm defect.

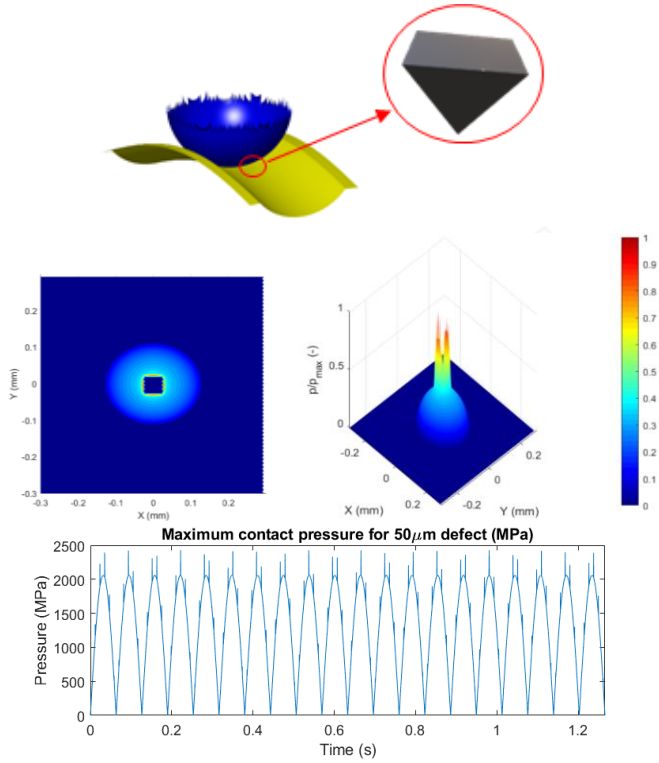

Figure 5. Contact pressure analysis for 50 µm defect.

2.3. Envelope analysis

Three main aspects of Fig. 4 can be pointed out. First, as expected from the time domain analysis of Fig. 2, the denoised signal was completely overlapped to the raw signal even in the frequency domain. Secondly, most of the harmonic content was in the low-medium frequency range. In this area, the faulty spectrum was considerably different from the signature spectrum. Then, the raw spectrum of the acquired signal did not show relevant contributions given by fault harmonics (x*BPFI*). As anticipated in the introduction to this work, such contributions are buried in the signal. Its shape is modelled in the frequency domain by resonances due to bursts, rather than by fault frequencies. Moreover, operating conditions typical of an industrial context did not exclude a-priori the presence of relevant noise and the manifestation of manifold sources of stationary and non-stationary disturbances. A Matlab® code was developed to perform the following tasks.

2.3.1. Pre-processing and enhancement of bearing signal

To enhance bearing signal and increase Signal to Noise Ratio (SNR), FK and SK were applied as pre-processing steps. The FK of the two accelerometers highlighted the optimal frequency bands for the signal demodulation. Furthermore, window lengths to be employed in the STFT for SK computation were selected on the basis of FK (Fig. 1 and Table 4). Signal windowing was performed with 80% overlap.

Table 4. Demodulation bands and window lengths.

Channel 1 (Radial Accelerometer)	
Demodulation band [Hz]	4800-5500
Window length (STFT) [Samples]	32
Channel 2 (Axial accelerometer)	
Demodulation band [Hz]	3800-4600
Window length (STFT) [Samples]	64

Figure 6 shows the signal Spectral Kurtosis and the 95% confidence interval for stationary Gaussian signals. The statistical thresholds are computed by taking into account that SK frequency distribution tends to a normal distribution with zero mean and variance $\frac{4}{N}$. Given the confidence level α and the quantile function $\Psi^{-1}(\alpha)$ of the standard normal distribution, the threshold th can be computed from Eq. (8).

$$th = \frac{2\Psi^{-1}(\alpha)}{\sqrt{N}} \qquad (8)$$

With respect to these boundaries, most of the harmonic content of the signal may be considered non-stationary, whereas the stationary part is contained in the low frequency range. The maximum kurtosis criterium was therefore adopted to enhance the non-stationary component of the signal, provided that the demodulation bands, thus estimated, were quite distanced from Nyquist limits. Signals Kurtosis (computed to find the value of 3 for Gaussian signals) before and after bandpass filtering is shown in Fig. 7.

Fig. 7 shows that the pre-processing step resulted very effective for the Channel 1 (vertical sensor) since the signal impulsiveness was enhanced by three times. Therefore, for the purposes of this analysis, the channel 1 was investigated. It is important to notice that, as long as impulsiveness is evaluated according to a SK criterion, peak values may be lower in frequency bands which encompass most of the impulsiveness than in others. Then, the authors of this work consider that the assessments on the signal diagnostic content based on peak values may be, in this case, misleading.

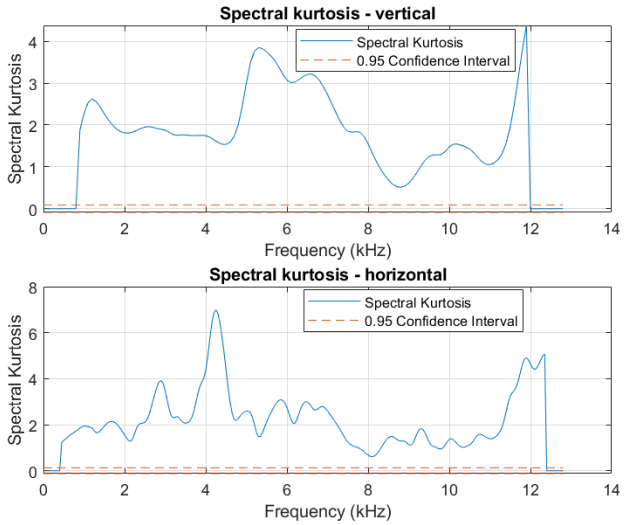

Figure 6. Spectral Kurtosis.

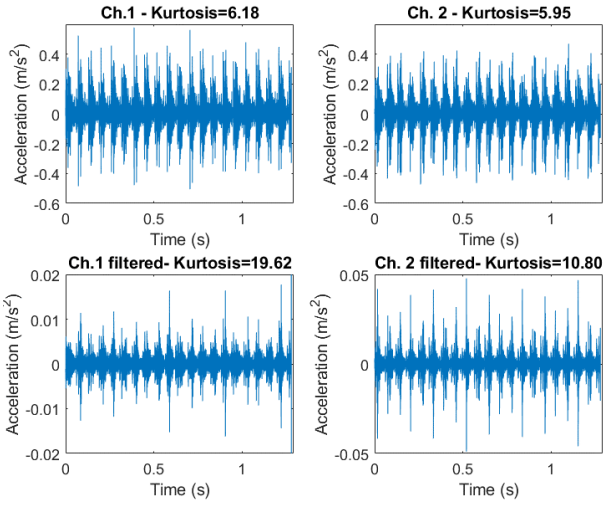

Figure 7. Signals Kurtosis.

2.3.2. Hilbert Transform

After the pre-processing was performed, the Hilbert transform was computed to demodulate the signal. Hilbert transformation $\tilde{x}(t)$ of the time signal $x(t)$ is defined as (Randall, 2011):

$$\tilde{x}(t) = \frac{1}{\pi}\int_{-\infty}^{+\infty} x(\tau)\frac{1}{t-\tau}d\tau \qquad (9)$$

Basically, it corresponds to a convolution which, in the frequency domain, acquires the form:

$$\tilde{X}(f) = X(f)(-j\, sgn(f)) \qquad (10)$$

where sgn is the sign function, and j the imaginary unit.

This is equivalent to apply FFT to the signal and shifting the phase of positive frequency contributes by $-\pi/2$ and of negative frequency contributes by $+\pi/2$. Practically, the amplitude demodulation with Hilbert transform can be achieved by computing the modulus of the *analytic signal*. This term refers to the complex time domain signal whose imaginary part is the Hilbert transform of the signal. The real part is represented by the original signal. The modulus of the *analytic signal* is the extracted envelope (Fig. 8).

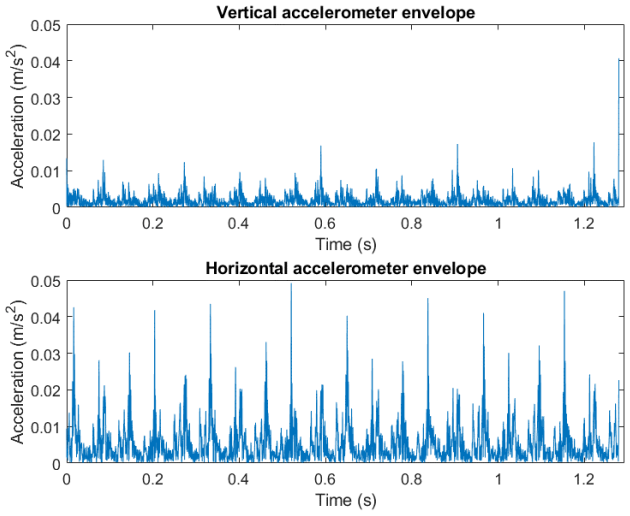

Figure 8. Signal Envelope.

Fig. 9 shows envelope spectra with different harmonic spacings. The first shaft speed component is prevalent. Nevertheless, differently from raw spectrum of Fig. 4, the influence of x*BPFI* harmonics is now detectable. Moreover, by comparing the signal spectrum with the envelope spectrum (Fig. 10), it is possible to notice the behavior of the first structural resonance whose contribution is flattened by the envelope extraction.

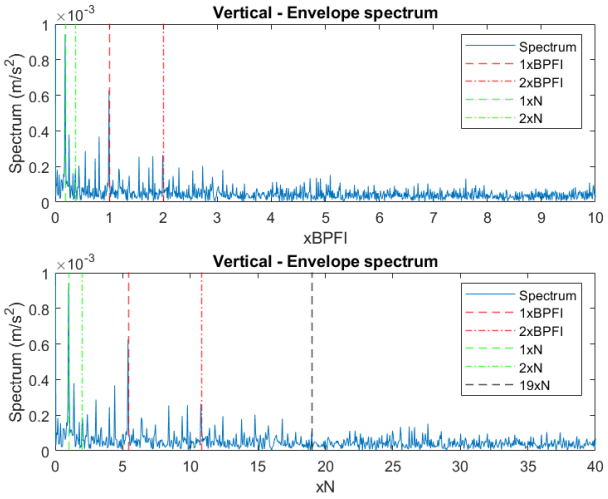

Figure 9. Envelope spectra for different harmonic spacing.

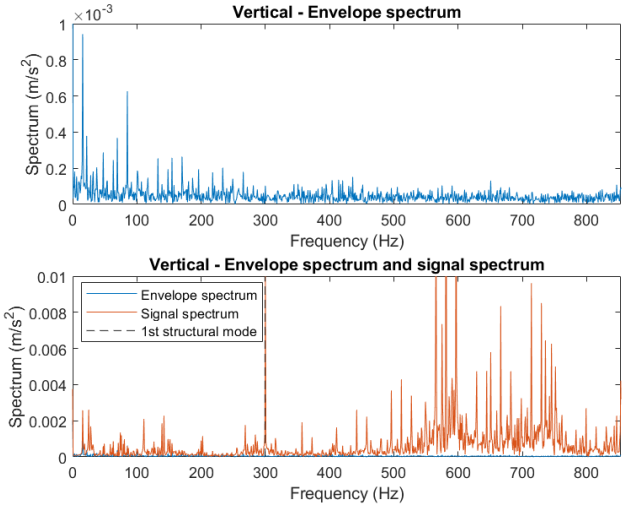

Figure 10. Envelope FFT and signal FFT.

2.4. Correlation of damage severity to the PSD

The envelope analysis was applied to the pressure signal to emphasize carrier and modulating frequencies for the different defect sizes. The pressure signal was demodulated in the same frequency band chosen for the channel 1 mainly for two reasons. First, the contact pressure and the vibration analysis wanted to be as much comparable as possible. Second, the frequency band suggested by the FK for the pressure signal was too high, given the narrowness of the resulting pressure peaks.

As a matter of fact, the spectrum of the pressure signal is dominated by discrete frequency components because it is deterministic. The spectra were normalized with respect to the corresponding maxima. Such dimensionless spectra make the pressure and the acceleration content comparable. Fig. 11 shows that fault information is hidden in the

pressure signal by the shaft speed harmonics whose contribution is prevalent with the mean part of the signal. Only the envelope analysis, indeed, highlighted the *xBPFI* harmonics with sidebands spaced at the shaft rotation frequency.

The method proposed in this study assumes that the x*BPFI* harmonics of the enveloped vibration signal somehow conceal information about the defect size. It was assumed that the energetic content of such harmonics was the significant feature. According to the authors, this is justified by the fact that, the more the energetic contribution given by such harmonics in the pressure signal resembles that given by the vibration signal, the more the size of the simulated defect is close to the real one. To this end, the modulus of the one-sided PSD was estimated by using FFT and the harmonic contributions given to the signal energy were analyzed.

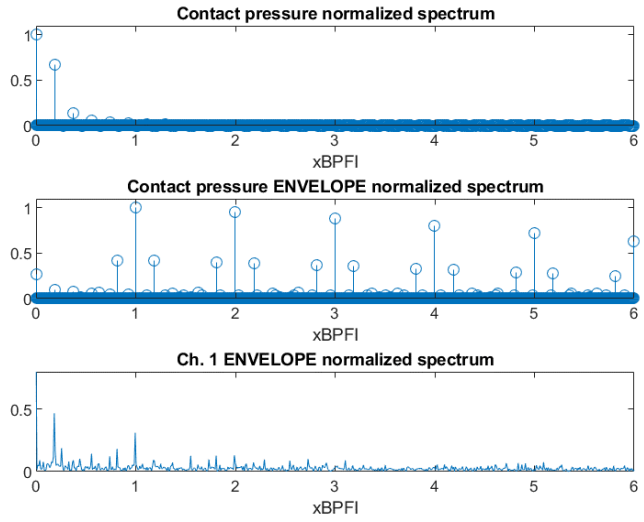

Figure 11. Contact pressure envelope, 20 µm defect.

Obviously, the total energies E_x, reported in Eq. (11), of the pressure signal and of the vibration signal were different. Insofar, the PSD resulting from signals with different physical units were not directly comparable. In order to overcome this limitation, the PSD were divided by the mean signal power, corresponding to the squared Root Mean Square value (RMS) of Eq. (12). This gave birth to the normalized quantity shown in Eq. (13). Thus, relative energetic contributions, rather than absolute, may be compared.

$$E_x = \int_{-\infty}^{+\infty} x^2(t)\, dt \qquad (11)$$

$$RMS^2 = \frac{E_x}{T} \qquad (12)$$

$$DPSD(f) = \frac{PSD(f)}{RMS^2} \qquad (13)$$

DPSD indicates a Dimensionless Power Spectral Density and PSD stands for the modulus of the one-sided Power Spectral Density. One of the properties of DPSD is that:

$$\int_{-\infty}^{+\infty} DPSD(f)\, df = 1 \qquad (14)$$

Strictly speaking, the integral of Eq. (14) is the dimensionless quantity, whereas the DPSD is measured in [Hz^{-1}]. However, the DPSD makes the energetic content of signals with different physical units comparable. For this reason, the adjective "dimensionless" is employed. Thanks to the DPSD, energetic frequency distributions coming from different type of signals can be matched. Finally, the DPSD of the vibration signal ($DPSD_x$) was subtracted from the DPSD of the pressure signal ($DPSD_p$) to assess differences in the relative energetic contributions. Relative Energetic Difference (RED) is given in Eq. (15). The followed methodology is summarized in Fig. 12.

$$RED(f) = \\ = DPSD_p(f) - DPSD_x(f) \qquad (15)$$

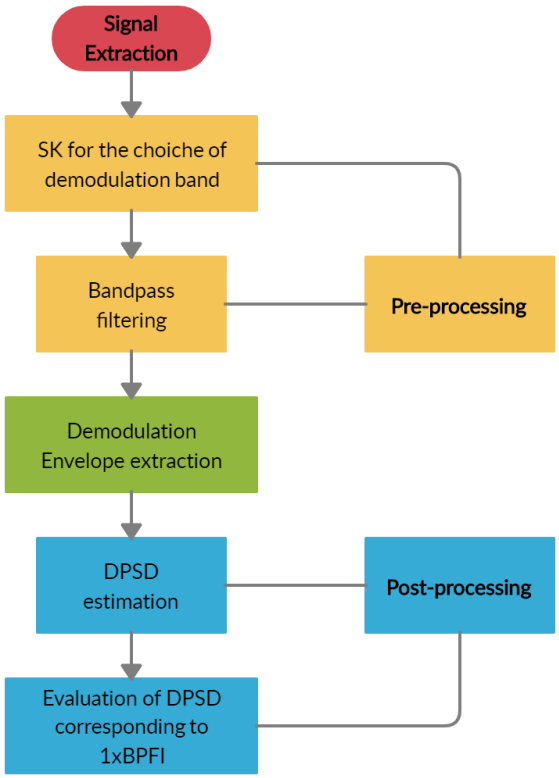

Figure 12. Analysis process.

DPSD is therefore useful for the purposes of this works to understand how the energetic content of the signal is distributed along the frequency domain. Moreover, this information is obtained relatively to the mean signal power, in a way that the integration of DPSD in a certain frequency

band gives as result the fraction of the signal power contained in such a band. It was not possible to analyze tachometer signal for performing angular resampling. Nevertheless, shaft speed harmonics can be distinguished in vibration spectra. Moreover, discrete frequency components were not removed to separate the deterministic part of the signal, but this was negligible for the purposes of this investigation. However, future work could include the discrete frequency removal by means of Time Synchronous Averaging (TSA) or Discrete Random Separation (DRS) (Randall & Antoni, 2011) in order to consider other components such as gears. Finally, further experimental data collection is required.

3. RESULTS AND DISCUSSION

The above model was applied for the different sizes in the contact pressure simulations. As already mentioned, this procedure intends to evaluate the effectiveness of health indicators, such as the x*BPFI* harmonics of the enveloped signal, when they are used as markers of damage severity. Relative Energetic Difference was introduced to compare the energetic contribution given by fault harmonics to signals which are not directly comparable, such as contact pressure and vibration signal. Then, high values of RED indicate that the relative energy associated to a certain frequency in the pressure signal, is quite different from the one associated to the same frequency in the vibration signal. Conversely, frequency bands showing low values of RED suggest a close relation between the relative energetic content of the vibration and the pressure signal in such bands.

Fig. 13 and Fig. 14 show the RED analysis performed both for the enveloped and the raw signals. Interestingly, significant values are found only at x*BPFI* harmonics as long as the signals are enveloped. Considering that the actual size of the defect is of units of micrometers, relevant differences are expected when the contact simulation is run for 20 µm (Fig. 13) and 50 µm (Fig. 14) defects but this did not occur for RED analysis of raw spectra. Therefore, RED analyses performed on the raw data suggest that non-demodulated signals have little informative content on defect size. This confirms the strength of envelope analysis not only for defect detection by means of health indicators, but even for the defect characterization. Although the exact shape and size of the real defect is unknown, RED evaluations for different simulated sizes call attention to the behavior of the $DPDS_p$ with respect to $DPSD_x$.

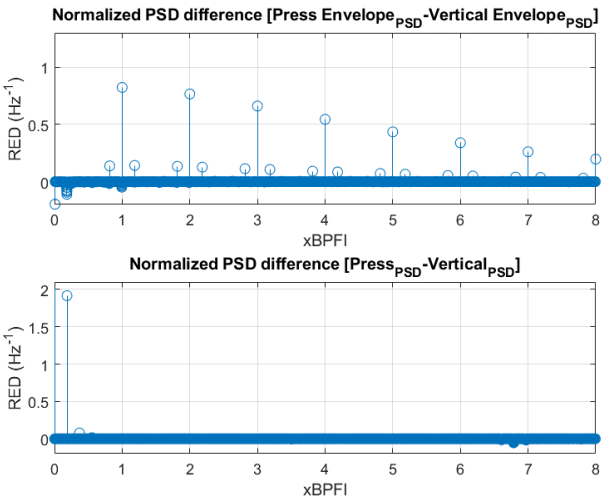

Figure 13. RED for 20 µm defect.

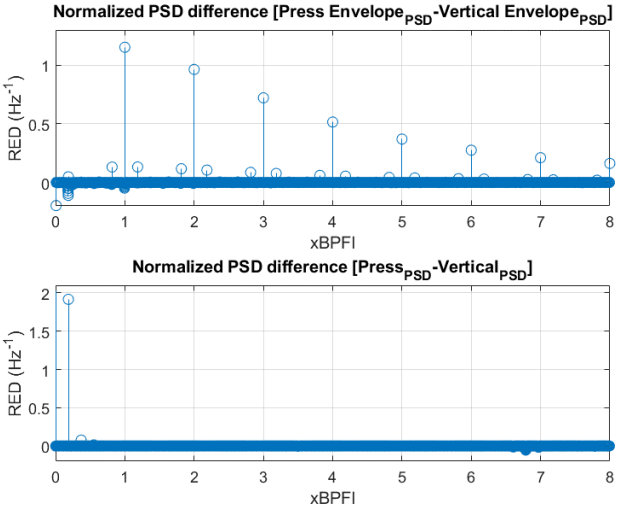

Figure 14. RED for 50 µm defect

Fig. 15 extends previous results showing the attitude of the first three *BPFI* harmonics. The relative energetic contribution of the above-mentioned pressure signal harmonics approaches the one of the vibration signal as the simulated size approaches the actual dimension, that is RED tends to zero. This is a remarkable outcome since it suggests a possible correlation between two different quantities also obtained in different modalities. However, these findings may be somewhat limited by the lack of further experimental activity for the examination of different defect shapes and appreciable sizes. The observed non-linear behavior occurs for all the harmonics but the 1x*BPFI* is slightly more sensitive. Furthermore, when the simulation is run for defects much larger than real ones, RED becomes less sensitive to further size variations. A possible explanation for this might be related to the interaction

between the size of the contact form and the size of the defect.

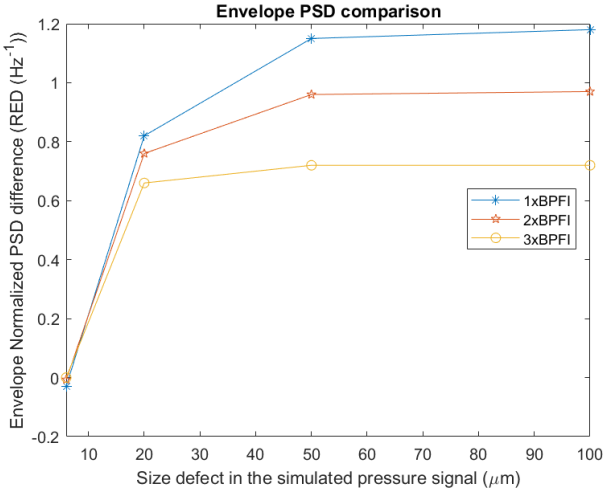

Figure 15. RED for 1-2-3x*BPFI* in the simulated size range.

Overall, these results indicate two main findings. The first is that the x*BPFI* harmonics of the enveloped contact pressure (especially the first) are able to describe the defect size. Secondly, when the relative energy contained in these components is compared to the vibration signal one, a correlation may be hypothesized. In particular, the behavior of x*BPFI* harmonics links the two spectra as long as they are properly processed. Hence, this work proposes a correlation and a procedure to emphasizes this link. Nevertheless, the relevance of the methodology with respect to other signal energy assessments must be further investigated. As a natural consequence, it might emerge that health indicators, such as relative energy linked to the 1x*BPFI* harmonic, also give insight into damage severity. Therefore DPSD relative to fault harmonics may be used to monitor the defect dimension. Practically, the procedure of Fig. 12 could be proposed to estimate damage severity in fault bearings. On the other hand, contact pressure analyses could be used to numerically simulate the behavior of the health indicators such as x*BPFI* harmonics with respect to different operating conditions.

4. CONCLUSION

The present study was designed to determine the attitude of non-Hertzian contact pressure towards damage severity and to relate this behavior to vibration signal. This investigation involved the use of CBM techniques such as envelope extraction for comparing numerical and experimental signals by using dimensionless quantities.

The results of this study show that the energetic contribution given by fault harmonics in the contact pressure provides indications on the damage severity. Moreover, dimensionless quantities enable comparisons with accelerometric signals. Starting from this comparison, a correlation between the two spectra is found. Namely, the relative contribution given by the fault harmonics to the signals power become similar. This supports the idea that the analyzed harmonics of the vibration signals are influenced by defect dimensions. Clearly, the same idea cannot be expressed if the absolute contributions (PSD) are compared, since they originate from different physical quantities. Interestingly, this correlation is not found for non-enveloped signals. Indeed, fault harmonics are not easily recognizable in raw spectra.

The most important limitations lie in the fact that further experiments are required. Then, further work is needed to establish whether this correlation is of a general nature and whether the analysis performed is actually a representative case. Indeed, this would mean that some features of the fault harmonics could be numerically replicated by using contact pressure analysis. Finally, further research might explore the effect of order tracking, discrete frequency separation and Wavelet Denoising on the enhancement of bearing signal and, consequently, on the comparison with the contact pressure spectrum.

NOMENCLATURE

$BPFI$	Ball passing frequency on the inner race
$BPFO$	Ball passing frequency on the outer race
$\boldsymbol{C}$	Influence coefficient matrix
d	Rolling element diameter
D	Distribution diameter
$DPSD$	Dimensionless Power Spectral Density
E_x	Signal energy
f	Frequency
f_r	Rotational frequency
F_s	Sampling frequency
FTF	Fundamental train frequency
$\boldsymbol{h}$	Gap function
j	Imaginary unit
$K(f)$	Spectral Kurtosis
n	Number of rolling elements
N	Number of samples
$\boldsymbol{p_n}$	Normal pressure
PSD	Power Spectral Density
RED	Relative Energetic Difference
RMS	Root Mean Square

sgn	Sign function
th	Statistical threshold
T	Acquisition time
$w(t)$	Time window
$x(t)$	Time signal
$\tilde{x}(t)$	Hilbert transform, time domain
$X(f,\tau)$	Signal time-frequency transform
$\tilde{X}(f)$	Hilbert transform, frequency domain
$\boldsymbol{\delta}$	Elastic deformation vector
Φ	Contact angle
Ψ^{-1}	Quantile function
ω	Spin speed

REFERENCES

Akansu, A. N., Haddadd, P. A., & Haddad, P. R. (2001). *Multiresolution signal decomposition: transforms, subbands, and wavelets.* Academic Press.

Al-Dossary, S., Hamzah, R. I. R., & Mba, D. (2009). Observations of changes in acoustic emission waveform for varying seeded defect sizes in a rolling element bearing. *Applied Acoustics*, *70*(1), 58–81. https://doi.org/10.1016/j.apacoust.2008.01.005

Al-Ghamd, A. M., & Mba, D. (2006). A comparative experimental study on the use of acoustic emission and vibration analysis for bearing defect identification and estimation of defect size. *Mechanical Systems and Signal Processing*, *20*(7), 1537–1571. https://doi.org/10.1016/j.ymssp.2004.10.013

Antoni, J. (2005). Blind separation of vibration components: Principles and demonstrations. *Mechanical Systems and Signal Processing*, *19*(6), 1166–1180. https://doi.org/10.1016/J.YMSSP.2005.08.008

Antoni, J. (2006). The spectral kurtosis: a useful tool for characterising non-stationary signals. *Mechanical Systems and Signal Processing*, *20*(2), 282–307. https://doi.org/10.1016/J.YMSSP.2004.09.001

Antoni, J. (2007). Fast computation of the kurtogram for the detection of transient faults. *Mechanical Systems and Signal Processing*, *21*(1), 108–124. https://doi.org/10.1016/J.YMSSP.2005.12.002

Antoni, J. (2015). The spectral kurtosis of nonstationary signals: Formalisation, some properties, and application. *European Signal Processing Conference*, *06-10-Sept*, 1167–1170.

Antoni, J., & Braun, S. (2005). Blind source separation. *Mechanical Systems and Signal Processing*, *19*(6), Special Issue.

Antoni, J., & Randall, R. B. (2006). The spectral kurtosis: application to the vibratory surveillance and diagnostics of rotating machines. *Mechanical Systems and Signal Processing*, *20*(2), 308–331. https://doi.org/10.1016/J.YMSSP.2004.09.002

Baccarini, L. M. R., Rocha e Silva, V. V., de Menezes, B. R., & Caminhas, W. M. (2011). SVM practical industrial application for mechanical faults diagnostic. *Expert Systems with Applications*, *38*(6), 6980–6984. https://doi.org/10.1016/J.ESWA.2010.12.017

Ben Ali, J., Saidi, L., Mouelhi, A., Chebel-Morello, B., & Fnaiech, F. (2015). Linear feature selection and classification using PNN and SFAM neural networks for a nearly online diagnosis of bearing naturally progressing degradations. *Engineering Applications of Artificial Intelligence*, *42*, 67–81. https://doi.org/10.1016/J.ENGAPPAI.2015.03.013

Bendat, J. S. (1991). *The Hilbert transform and applications to correlation measurements*.

Bonnardot, F., & Randall, R. B. (2004). Enanched unsupervised noise cancellation using angular resampling for planetary bearing fault diagnosis. *International Journal of Acoustics and Vibration*, *9*(2), 51–60.

Borghesani, P., Pennacchi, P., & Chatterton, S. (2014). The relationship between kurtosis- and envelope-based indexes for the diagnostic of rolling element bearings. *Mechanical Systems and Signal Processing*, *43*(1–2), 25–43. https://doi.org/10.1016/J.YMSSP.2013.10.007

Burchill, R. F. (1973). Resonant structure techniques for bearing fault analysis. *National Bureau of Standards NBSIR*, *73*.

Burchill, R. F., John, L. F., & Wilson, D. S. (1973). New machinery health diagnostic techniques using high-frequency biration. *SAE Technical Paper*.

Chen, A., & Kurfess, T. R. (2018). A new model for rolling element bearing defect size estimation. *Measurement: Journal of the International Measurement Confederation*, *114*(May 2017), 144–149. https://doi.org/10.1016/j.measurement.2017.09.018

Daga, A. P., Fasana, A., Marchesiello, S., & Garibaldi, L. (2019). The Politecnico di Torino rolling bearing test rig: Description and analysis of open access data. *Mechanical Systems and Signal Processing*, *120*, 252–273. https://doi.org/10.1016/j.ymssp.2018.10.010

Darlow, M., & Badgley, R. H. (1975). Early detection of defects in rolling-element bearings. *SAE Technical Paper*.

Delprete, C., Brusa, E., Rosso, C., & Bruzzone, F. (2020).

Bearing Health Monitoring Based on the Orthogonal Empirical Mode Decomposition. *Shock and Vibration*, *2020*. https://doi.org/10.1155/2020/8761278

Delprete, C., Milanesio, M., & Rosso, C. (2005). Rolling bearings monitoring and damage detection methodology. *Applied Mechanics and Materials*, *3–4*, 293–302. https://doi.org/10.4028/www.scientific.net/AMM.3-4.293

Donoho, D. L., & Johnstone, J. M. (1994). Ideal spatial adaptation by wavelet shrinkage. *Biometrika*, *81*(3), 425–455. https://doi.org/10.1093/biomet/81.3.425

Genta, G. (2007). *Dynamics of rotating systems*. Springer Science & Business Media.

Genta, G., Delprete, C., & Brusa, E. (1999). Some considerations on the basic assumptions in rotordynamics. *Journal of Sound and Vibration*, *227*(3), 611–645.

Guo, Y., Liu, T.-W., Na, J., & Fung, R.-F. (2012). Envelope order tracking for fault detection in rolling element bearings. *Journal of Sound and Vibration*, *331*(25), 5644–5654. https://doi.org/10.1016/J.JSV.2012.07.026

Harting, D. R. (1978). Demodulated resonance analysis-A powerful incipient failure detection technique. *ISAT*, *17*(1), 35–40.

Herp, J., Ramezani, M. H., Bach-Andersen, M., Pedersen, N. L., & Nadimi, E. S. (2018). Bayesian state prediction of wind turbine bearing failure. *Renewable Energy*, *116*, 164–172. https://doi.org/10.1016/j.renene.2017.02.069

Hong, H., & Liang, M. (2009). Fault severity assessment for rolling element bearings using the Lempel-Ziv complexity and continuous wavelet transform. *Journal of Sound and Vibration*, *320*(1–2), 452–468. https://doi.org/10.1016/j.jsv.2008.07.011

Jin, X., & Chow, T. W. S. (2013). Anomaly detection of cooling fan and fault classification of induction motor using Mahalanobis-Taguchi system. *Expert Systems with Applications*, *40*(15), 5787–5795. https://doi.org/10.1016/j.eswa.2013.04.024

Jin, X., Wang, Y., Chow, T. W. S., & Sun, Y. (2017). MD-based approaches for system health monitoring: A review. *IET Science, Measurement and Technology*, *11*(4), 371–379. https://doi.org/10.1049/iet-smt.2016.0340

Johnson, K. L. (1987). *Contact Mechanics*. Cambridge university press.

Kalker, J. J. (2013). *Three-dimensional elastic bodies in rolling contact*. Springer Science & Business Media.

Kankar, P. K., Sharma, S. C., & Harsha, S. P. (2011). Rolling element bearing fault diagnosis using wavelet transform. *Neurocomputing*, *74*(10), 1638–1645. https://doi.org/10.1016/j.neucom.2011.01.021

Lin, J., & Qu, L. (2000). Feature extraction based on morlet wavelet and its application for mechanical fault diagnosis. *Journal of Sound and Vibration*, *234*(1), 135–148. https://doi.org/10.1006/jsvi.2000.2864

Liu, Z., Cao, H., Chen, X., He, Z., & Shen, Z. (2013). Multi-fault classification based on wavelet SVM with PSO algorithm to analyze vibration signals from rolling element bearings. *Neurocomputing*, *99*, 399–410. https://doi.org/10.1016/J.NEUCOM.2012.07.019

Mauricio, A., Smith, W., Randall, R. B., Antoni, J., & Gryllias, K. (2018). Cyclostationary-based tools for bearing diagnostics. *Proceedings of ISMA 2018 - International Conference on Noise and Vibration Engineering and USD 2018 - International Conference on Uncertainty in Structural Dynamics*, 905–918.

Mba, D. (2008). The use of acoustic emission for estimation of bearing defect size. *Journal of Failure Analysis and Prevention*, *8*(2), 188–192. https://doi.org/10.1007/s11668-008-9119-8

McCormick, A. C., & Nandi, A. K. (1998). Cyclostationarity in Rotating Machine Vibrations 1 Introduction 2 Wide-sense Cyclostationarity. *Mechanical Systems and Signal Processing*, *12*(2), 225–242.

McFadden, P. D. (1989). Interpolation techniques for time domain averaging of gear vibration. *Mechanical Systems and Signal Processing*, *3*(1), 87–97. https://doi.org/10.1016/0888-3270(89)90024-1

McFadden, P. D., & Smith, J. D. (1984a). Model for the vibration produced by a single point defect in a rolling element bearing. *Journal of Sound and Vibration*, *96*(1), 69–82. https://doi.org/10.1016/0022-460X(84)90595-9

McFadden, P. D., & Smith, J. D. (1984b). Vibration monitoring of rolling element bearings by the high-frequency resonance technique — a review. *Tribology International*, *17*(1), 3–10. https://doi.org/10.1016/0301-679X(84)90076-8

Mohanty, A. R. (2014). Machinery condition monitoring: Principles and practices. In *Machinery Condition Monitoring: Principles and Practices*.

Peng, Z. K., & Chu, F. L. (2004). Application of the wavelet transform in machine condition monitoring and fault diagnostics: A review with bibliography. *Mechanical Systems and Signal Processing*, *18*(2), 199–221. https://doi.org/10.1016/S0888-3270(03)00075-X

Pinheiro, A. A., Brandao, I. M., & Da Costa, C. (2019). Vibration Analysis in Turbomachines Using Machine Learning Techniques. *European Journal of Engineering Research and Science*, *4*(2), 12–16. https://doi.org/10.24018/ejers.2019.4.2.1128

Potter, R., & Gribler, M. (1989). Computed order tracking obsoletes older methods. *SAE Transactions*, 1099–1103.

Qiu, H., Lee, J., Lin, J., & Yu, G. (2006). Wavelet filter-based weak signature detection method and its application on rolling element bearing prognostics. *Journal of Sound and Vibration*, *289*(4–5), 1066–1090. https://doi.org/10.1016/j.jsv.2005.03.007

Randall, R. B. (2011). Vibration-based condition monitoring: industrial, aerospace and automotive applications. In *Mechanisms and Machine Science*. John Wiley & Sons. https://doi.org/10.1007/978-94-007-6422-4_11

Randall, R. B., & Antoni, J. (2011). Rolling element bearing diagnostics-A tutorial. *Mechanical Systems and Signal Processing*, *25*(2), 485–520. https://doi.org/10.1016/j.ymssp.2010.07.017

Randall, R. B., Antoni, J., & Chobsaard, S. (2001). The relationship between spectral correlation and envelope analysis in the diagnostics of bearing faults and other cyclostationary machine signals. *Mechanical Systems and Signal Processing*, *15*(5), 945–962. https://doi.org/10.1006/mssp.2001.1415

Rubini, R., & Meneghetti, U. (2001). Application of the envelope and wavelet transform analyses for the diagnosis of incipient faults in ball bearings. *Mechanical Systems and Signal Processing*, *15*(2), 287–302. https://doi.org/10.1006/MSSP.2000.1330

Sawalhi, N. (2007). *Diagnostics, Prognostics and Fault Simulation. April*. https://www.unsworks.unsw.edu.au/permalink/f/a5fmj0/unsworks_1509

Sawalhi, N., & Randall, R. B. (2008). Semi-automated bearing diagnostic-three case studies. *Non Destrcutive Testing Australia*, *45*(2), 59.

Shakya, P., Kulkarni, M. S., & Darpe, A. K. (2015). Bearing diagnosis based on Mahalanobis-Taguchi-Gram-Schmidt method. *Journal of Sound and Vibration*, *337*, 342–362. https://doi.org/10.1016/j.jsv.2014.10.034

Shao, H., Jiang, H., Wang, F., & Wang, Y. (2017). Rolling bearing fault diagnosis using adaptive deep belief network with dual-tree complex wavelet packet. *ISA Transactions*, *69*, 187–201. https://doi.org/10.1016/J.ISATRA.2017.03.017

Tabrizi, A., Garibaldi, L., Fasana, A., & Marchesiello, S. (2015a). A novel feature extraction for anomaly detection of roller bearings based on performance improved ensemble empirical mode decomposition and Teager-Kaiser energy operator. *International Journal of Prognostics and Health Management*, *6*, 1–10.

Tabrizi, A., Garibaldi, L., Fasana, A., & Marchesiello, S. (2015b). Early damage detection of roller bearings using wavelet packet decomposition, ensemble empirical mode decomposition and support vector machine. *Meccanica*, *50*(3), 865–874. https://doi.org/10.1007/s11012-014-9968-z

Wang, D., Tse, P. W., & Tsui, K.-L. (2013). An enhanced Kurtogram method for fault diagnosis of rolling element bearings. *Mechanical Systems and Signal Processing*, *35*(1–2), 176–199. https://doi.org/10.1016/J.YMSSP.2012.10.003

Wang, D., Tsui, K.-L., & Miao, Q. (2018). Prognostics and Health Management: A Review of Vibration Based Bearing and Gear Health Indicators. *IEEE Access*, *6*, 665–676. https://doi.org/10.1109/ACCESS.2017.2774261

Wang, X. Y., Makis, V., & Yang, M. (2010). A wavelet approach to fault diagnosis of a gearbox under varying load conditions. *Journal of Sound and Vibration*, *329*(9), 1570–1585. https://doi.org/10.1016/j.jsv.2009.11.010

Wang, Y., He, Z., & Zi, Y. (2010). Enhancement of signal denoising and multiple fault signatures detecting in rotating machinery using dual-tree complex wavelet transform. *Mechanical Systems and Signal Processing*, *24*(1), 119–137. https://doi.org/10.1016/j.ymssp.2009.06.015

Welch, P. D. (1975). The Use of Fast Fourier Transform for the Estimation of Power Spectra. *Digital Signal Processing*, *2*, 532–574.

Widodo, A., & Yang, B.-S. (2007). Support vector machine in machine condition monitoring and fault diagnosis. *Mechanical Systems and Signal Processing*, *21*(6), 2560–2574. https://doi.org/10.1016/J.YMSSP.2006.12.007

Wriggers, P. (2002). *Computational contact mechanics*. Springer.

Yu, D., Cheng, J., & Yang, Y. (2005). Application of EMD method and Hilbert spectrum to the fault diagnosis of roller bearings. *Mechanical Systems and Signal Processing*, *19*(2), 259–270. https://doi.org/10.1016/S0888-3270(03)00099-2

BIOGRAPHIES

Eugenio Brusa was born in Torino in 1969. He graduated as Aeronautical Engineer at the Politecnico di Torino in 1993. He received the Ph.D in Machine Design in 1997 at the Politecnico di Torino with a thesis on the design of an active stabilization of free rotors, within the frame of a project of the Italian Space Agency. He was Assistant Professor of Machine Design in Torino since 1998 to 2001 and Associate Professor at University of Udine since 2001 to 2008. Since 2008 he belongs to the Dept. of Mechanical and Aerospace Engineering of the Politecnico di Torino. In 2010 he was appointed Full Professor of Machine Design, running in this role in 2013. Currently he is Director of the Doctorate School of the Politecnico di Torino. His research activities concern structural mechanical design, structural mechatronics, micromechatronics and Model Based Systems Engineering (MBSE). He founded an currently leads a research group active within the Industrial System Engineering and Design applied to industry, smart manufacturing and products. He wrote more than 210 papers either published on scientific journals or presented to international conferences. He is co-author of some books on Microsystem Mechanical Design, MEMS and structural mechatronics. He taught Structural Mechatronics, Structural Micromechatronics and Rotor dynamics and control as invited lecturer in short courses and seminars. He is member of the ASME (American Society of Mechanical Engineers), INCOSE (International Council of Systems Engineers) and AIAS (Italian Society for Stress Analysis).

Fabio Bruzzone was born in Alba in 1988. He received M. Sc in 2016 in mechanical engineering at the Politecnico di Torino university and is in the process of obtaining his Ph.D in the same field at the same university. His Ph.D dissertation focuses on novel methods for the quasi-static and dynamic analysis of compliant gears with a nonlinear and non-Hertzian approach. He is a member of the Industrial System Engineering and Design and is practical lecturer of different courses in the same university. He is co-founder of Rotor, a start-up commercializing an innovative vertical axis wind turbine. He is also co-founder and Chief Software Engineer at GeDy TrAss, a spin-off of Politecnico di Torino commercializing an innovative software for the detailed analysis of mechanical transmissions.

Cristiana Delprete was born in Cuneo in 1963. She graduated as Mechanical Engineer at the Politecnico di Torino in 1988. She received the Ph.D in Applied Mechanics, Mechanical Systems and Structures at the Dept. of Mechanics of the same university in 1993 with a thesis on the design and experimental test of first Italian spindle on active magnetic bearings. Since 1991 to 1998 she was Assistant Professor of Machine Design at Politecnico di Torino. She was Technical Coordinator of the Interdepartmental Laboratory of Mechatronics at the Politecnico di Torino since 1993 to 1996. Since 1998 to 2017 she was Associate Professor of Machine Design at the same university. In 2017 she was appointed Full Professor of Machine Design. Since 2009 she is Faculty Advisor of the Policumbert Student Team of the Politecnico di Torino. Her research activity focuses on virtual design and numerical simulation of mechanical and engine subsystems, experimental characterization of materials of industrial interest, analytical and numerical modelling for estimating the residual life, dynamic behavior of rotating machinery, monitoring and diagnostic techniques for evaluating damage, innovative heat treatments, design, construction and testing of human powered vehicles (HPV). Since 2001 she leaded the Research Group on Design of Powertrain and Engine Components: Materials, Testing and Simulation at Politecnico di Torino. She wrote more than 230 papers published in international journals and conference proceedings and 3 patents. Currently, she leads the research group of Industrial System Engineering and Design at Politecnico di Torino. She is member of the Engineers SAE (Society of Automotive) and AIAS (Italian Society for Stress Analysis). She is active in several scientific collaborations with some international universities.

Luigi Gianpio Di Maggio was born in Taranto in 1994. He graduated in mechanical engineering B.Sc. in 2016 and received M.Sc in 2019 at the Politecnico di Torino with a thesis on analytical and numerical methods for assessing the fatigue life in threaded bores of engine components. Since 2019 he is a Ph.D student at the same university in the research group of Industrial System Engineering and Design. His research “Digitalized Virtual Engineering and Testing of Lean Rotating Systems” focuses on the study of prompt condition monitoring, structural health diagnosis and failure prevention in industrial rotating systems.

Carlo Rosso was born in Savona in 1975. He graduated as Mechanical Engineer at the Politecnico di Torino in 2001, he holds a PhD in Machine design and Construction from Politecnico di Torino in the 2005, he is Associate Professor in Machine Design at the Department of Mechanical and Aerospace Engineering of Politecnico di Torino since 2016. His main research topics are focusing on the dynamics of mechanical components with particular attention for the gears and the metal replacement in automotive industries. In particular he is focused on the design and life assessment of gearbox components with emphasis on gears and bearings. He is author of 4 patents and founder of two start-ups and one of this is Spin-Off of Politecnico di Torino. He is co-author of 50+ pier-reviewed publications about machine design topics. He has a good relationship with the industrial tissue of the Piedmont region and he had signed industrial research agreements for more than 920000 €. He is active member of SAE international and SEM.